STEM CELLS TRANSLATIONAL MEDICINE®

TISSUE ENGINEERING AND REGENERATIVE MEDICINE

Three Years After Transplants in Human Mandibles, Histological and In-Line Holotomography Revealed That Stem Cells Regenerated a Compact Rather Than a Spongy Bone: Biological and Clinical Implications

ALESSANDRA GIULIANI,[a,*] ADRIAN MANESCU,[a,*] MAX LANGER,[b,c,d] FRANCO RUSTICHELLI,[a] VINCENZO DESIDERIO,[e,f] FRANCESCA PAINO,[f] ALFREDO DE ROSA,[g] LUIGI LAINO,[g] RICCARDO D'AQUINO,[g] VIRGINIA TIRINO,[f] GIANPAOLO PAPACCIO[f]

[a]Dipartimento di Scienze Cliniche e Odontostomatologiche, Sezione di Biochimica, Biologia e Fisica, Università Politecnica delle Marche, Ancona, Italy; [b]Creatis, INSA-Lyon, Lyon, France; [c]Université CB, Lyon, France; [d]European Synchrotron Radiation Facility, Grenoble, France; [e]Department of Computational Medicine and Bioinformatics, Center for Organogenesis of Complex Tissues, University of Michigan, Ann Arbor, Michigan, USA; [f]Dipartimento di Medicina Sperimentale, Sezione di Istologia e Medicina Rigenerativa, Seconda Università degli Studi di Napoli, Naples, Italy; [g]Dipartimento di Odontostomatologia, Seconda Università degli Studi di Napoli, Naples, Italy

[*]Contributed equally as first authors.

Correspondence: Gianpaolo Papaccio, M.D., Ph.D., Department of Experimental Medicine, Section of Histology, Laboratory of Tissue Engineering and Regenerative Medicine, Second University of Naples, via L. Armanni 5-80138 Naples (I), Italy. Telephone: 39-08-15666015/7720/7715; Fax: 39-08-15666014; E-Mail: gianpaolo.papaccio@unina2.it

Received October 18, 2012; accepted for publication January 24, 2013; first published online in SCTM *EXPRESS* March 15, 2013.

1066-5099/2013/$20.00/0

http://dx.doi.org/10.5966/sctm.2012-0136

Key Words. Clinical trials • Differentiation • Stem cell transplantation • Tissue regeneration • Bone

ABSTRACT

Mesenchymal stem cells deriving from dental pulp differentiate into osteoblasts capable of producing bone. In previous studies, we extensively demonstrated that, when seeded on collagen I scaffolds, these cells can be conveniently used for the repair of human mandible defects. Here, we assess the stability and quality of the regenerated bone and vessel network 3 years after the grafting intervention, with conventional procedures and in-line holotomography, an advanced phase-imaging method using synchrotron radiation that offers improved sensitivity toward low-absorbing structures. We found that the regenerated tissue from the graft sites was composed of a fully compact bone with a higher matrix density than control human alveolar spongy bone from the same patient. Thus, the regenerated bone, being entirely compact, is completely different from normal alveolar bone. Although the bone regenerated at the graft sites is not of the proper type found in the mandible, it does seem to have a positive clinical impact. In fact, it creates steadier mandibles, may well increase implant stability, and, additionally, may improve resistance to mechanical, physical, chemical, and pharmacological agents. STEM CELLS TRANSLATIONAL MEDICINE *2013;2:316–324*

INTRODUCTION

Dental pulp stem cells (DPSCs) are mesenchymal stem cells embryologically derived from both neural crest and mesenchyme, like many other stem cells of the oro-maxillo-facial (OMF) body area, including dental follicle cells [1–5]. These cells display a variety of characteristics and differentiation potentials. In our previous studies, we demonstrated that DPSCs isolated from dental pulp coexpress CD34 and CD117, proliferate extensively, have a long lifespan, and maintain their multipotency for many generations [3, 6–9]. In addition, DPSCs are capable of differentiating into adipocytes, chondrocytes, and myocytes when cultured in adipo-chondro-myogenic media and into osteoblasts and bone when cultured in standard medium supplemented with 20% fetal bovine serum but no specific osteogenic morphogens and are capable of forming a complete and well-vascularized lamellar bone after grafting in immunosuppressed rats [1, 3]. The quality and quantity of the regenerated bone formed from DPSCs were demonstrated both in vitro and in vivo in experiments using stem cells and biomaterials [1, 3, 9–11].

Bone repair and regeneration are of major interest not only for the OMF area but also for the body in general. Bone loss is caused by many (congenital and degenerative) diseases, traumas, and surgical procedures; it leads to problems in functionality and is having an ever-increasing social impact, especially for the elderly. Thus, dental pulp is an interesting and potentially important source of ready-for-use autologous stem/progenitor cells for therapies aimed at the repair/regeneration of bone defects.

In our clinical studies on OMF bone repair, we used a biocomplex made of up DPSCs seeded onto an equine collagen I-based sponge scaffold. The enrolled patients had significant bone loss (alveolar loss of more than 7 mm in height, without walls) caused by extraction of their third molars. Six months from the intervention, we found that DPSCs were responsible for optimal vertical repair of the damage area and completely restored the periodontal tissue up to the second molars; regenerated bone was still evident 1 year

from grafting [10]. This first clinical study suggested that DPSCs may be useful for tissue repair and/or regeneration.

In the present study, we report a 3-year follow-up of these patients and explore how to better understand the stability and the characteristics of regenerated bone with the novel synchrotron radiation-based holotomography technique. More conventional microscopy assays for the visualization of tissue-rebuilding processes, such as light, fluorescence, scanning, and transmission electron microscopy, are useful but are limited to producing two-dimensional (2D) local information or require laborious three-dimensional (3D) reconstruction of serial sections [12]. Bone structure and remodeling are therefore traditionally evaluated by x-ray radiography, which has a low cost, has widespread availability, and is flexible. However, the intrinsic limitations of the physical properties of this method and the number of variables involved (exposure setting, beam source-film distance, x-ray filtration, etc.) means that analytical and diagnostic imaging techniques such as x-ray microtomography (μCT) are now preferred; in fact, these techniques can deliver additional information for the investigation of in vivo tissue-engineering constructs and contribute decisively to the understanding of the biological processes involved [13]. With the use of synchrotron radiation, moreover, tomographic imaging can acquire a pixel resolution of as little as 270 nm and thus is comparable to light microscopy.

Traditionally, absorption imaging with μCT in medical applications is conducted with almost no distance between sample and detector. Homogeneous materials with a low attenuation coefficient or heterogeneous materials with a narrow range of attenuation coefficients will produce insufficient contrast for absorption imaging [14]. For such materials, the imaging quality can be enhanced through the use of phase contrast tomography (PCT) with an increased distance between sample and detector [15]. In addition, whereas PCT is based on a single distance between the detector and the sample, holotomography (HT) involves imaging at several distances and then combining the phase-shift information to generate 3D reconstructions [16]. HT is helpful when the material of interest has very small variations in attenuation coefficients, which lead to unsatisfactory imaging results even with phase-contrast techniques. This is the case for fully and partially mineralized bones, such as that created by a regeneration process deriving from engrafted stem cells.

Here, through the use of traditional methods and synchrotron radiation-based HT (SR-HT), we show that 3 years from surgery the regenerated tissue was a fully compact bone rather than the spongy alveolar type normal for this area. Although not physiologic, this bone type conferred more stability to the mandible and may provide patients with interesting treatment opportunities.

Materials and Methods

Ethical Committee

All procedures complied with Internal Ethical Committee guidelines, approved on June 12, 2005 (Second University of Naples [SUN] Internal Registry: Experimentation #914, Bone Repair Using Stem Cells). The patients enrolled in this study signed an informed consent form drafted by SUN researchers following instructions from the SUN Internal Ethical Committee.

Cell Isolation and Engraftment

Full details of the surgical and other procedures used have been previously published [10]. Briefly, patients ($n = 7$) were prepared for surgery by decontamination of the oral cavity with chlorhexidine before extraction of the lower (mandibular) impacted third molars with the following standard procedure. After making a horizontal incision in the gum, the muco-periosteal flap was reflected, and the bone covering the tooth was removed using a round bur. The area was irrigated with a steady stream of saline solution until the crown was entirely exposed. When the oral surgeon was not able to extract the whole tooth at one time, a groove was created vertically (along the long axis) at the cervical line, using a fissure bur, in order to separate the crown from the root. The groove created by the bur was not deep, since the mandibular canal is often found in close proximity to the tooth and injuring or severing the inferior alveolar nerve must be avoided. A straight elevator was placed in the groove and used to separate the crown from the root, with a rotary movement. The crown was removed separately, using the same elevator, with a rotary movement upward; the root was then easily removed using a straight or angled elevator, the blade end of which was placed on a purchase point created on the buccal side of the root. In the case of teeth with multiple roots, the crown was sectioned and removed as above described. Afterward, if the roots of the impacted tooth were separated during crown sectioning, they were easily removed in succession, starting with the distal root and moving on to the mesial root.

After smoothing the bone, the area was irrigated with saline solution, and the distal root of the second molar was planned with a Gracey curette. All necrotic tissue was removed. The pulp chamber was opened using a surgical drill, and the pulp was collected using a Gracey curette. The pulp was then rinsed in 1.5 ml of saline solution and mechanically dissociated using previously described procedures [3, 6, 10].

In order to isolate stem cells from whole pulp, the cells were incubated with CD34-conjugated microbeads for 30 minutes at 4°C. After passage through a magnetically activated cell-sorting column (Miltenyi Biotec, Bergisch Gladbach, Germany, http://www.miltenyibiotec.com), the collected $CD34^+$ stem cells were gently seeded with a syringe onto a collagen sponge scaffold (Gingistat; Vebas, San Giuliano Milanese, Italy, http://www.gaba-info.it). This sponge-cell implant was used to fill the space left by the extraction procedure (test or T site). Sponge without cells was used to fill the control (C) site. A flap of gum was then sutured over the area in order to avoid any contact with the oral cavity. Additional sutures were placed at the distal portion of the second molar, at the interdental papillae, and at the posterior end of the incision. For both sites (C and T sites), a replacement jig was placed to ensure correct localization for sample withdrawal.

Patient Follow-Up

The SUN Ethical Committee permitted a maximum of four x-ray orthopantomographies per year and a maximum of eight endo-oral x-rays per year on each patient. After the first year of grafting, all patients were visited once every 6 months, up to the 3rd year. During visits, clinical observations and x-rays were performed. All patients were routinely controlled for the presence of viral infections, including cytomegalovirus, Epstein-Barr virus, human herpes virus 8, poliomavirus, human T-cell lymphotrophic virus 1/2, and influenza viruses.

Three years after grafting, the following samples were obtained from all patients with mini-invasive surgery in order to avoid any potential loss of periodontal tissue: mandible regenerated as previously reported [10], hereafter called "human in vivo stem cell (SC)-treated mandible" (corresponding to the T site), and normal cortical mandible extracted from the contralateral side of each patient, as an internal control, hereafter called "human mandible control" (corresponding to the C site). The samples were collected with an Elcomed drill (W&H Dentalwerk, Bürmoos, Austria, http://www.wh.com) using the replacement jigs that had been previously inserted. The drill was capable of measuring bone resistance in Newton centimeters (N·cm). The bone samples obtained were 2.8–3.0 mm in diameter and 10–11 mm in length. Samples from six patients were processed for histological analyses, and those from one patient were analyzed with SR-HT. Before and after collection, the patients were clinically examined by physicians and underwent routine x-ray analysis, following the follow-up protocol.

Hematoxylin-Eosin and Mallory's Trichrome Staining

Human in vivo SC-treated mandible and human mandible control biopsies were decalcified using 10% EDTA in distilled water for 2 months and then fixed with 4% paraformaldehyde for 24 hours at 4°C, washed in phosphate-buffered saline (PBS), incubated in 30% sucrose for 3 days, washed in PBS, and then embedded in an optimal cutting temperature compound (Bio-Optica, Milan, Italy, http://www.bio-optica.it).

For hematoxylin-eosin staining, the sections were cut into 5-μm-thick slices, washed in distilled water for 10 minutes, and placed in hematoxylin for 5 minutes. After three washes in distilled water, the samples were placed in spring water for 20 minutes. The samples were then placed in acetic acid-acidified eosin for 30 seconds. Finally, they were passed through a graded sequence of alcohols (95°, 75°, and 95°) and mounted with DPX mounting medium.

For Mallory's trichrome staining, the sections were stained in acid fuchsine for 1 minutes, then methylene blue-orange G and oxalic acid solution for 25 minutes, and finally phosphotungstic acid for 15 minutes: collagen fibrils are colored in blue, nuclei in red, and cytoplasm in orange. After dehydration in a graded series of alcohols (95°, 75°, and 95°), they were mounted with DPX.

Bone Histomorphometry

Four-micrometer sections originating from all the regions of the retrieved bone samples ($n = 6$ patients) were processed for histomorphometrical analysis and observed by two different researchers in a blind manner. Digital images were acquired and captured at $\times$100 magnification with an Olympus light microscope. For each area of interest, the bone volume (BV) was calculated both as a percentage of the total tissue volume (TV) and in μm^3, whereas bone surface/bone volume (BS/BV) was calculated in mm^{-1}. Marrow star space volume (MSV) was calculated as follows: MSV = (volume of marrow space/volume of trabeculae and marrow) $\times$ 100. All analyses and measurements were performed with ImageJ software, version 3.

Synchrotron X-Ray Holotomography

Fresh biopsies obtained from one patient were cleaned with a fine brush and placed in a 6:3:1 mixture of 80% ethanol, 35% formaldehyde, and 100% acetic acid for 24 hours. They were then dehydrated in a graded ethanol series (70%, 75%, 80%, 85%, 90%, 95%, and 100%) with three changes at each concentration and 10 minutes between steps and dried under a hood overnight before HT acquisition. HT was performed with an ID19 Beamline (European Synchrotron Radiation Facility [ESRF], Grenoble, France) using a beam energy of 20 keV. The radiographs were recorded with a cooled CCD camera (ESRF FReLoN) with a 14-bit dynamic range at 2,048 $\times$ 2,048 pixels and with a pixel size of 678 nm. We recorded 1,500 projections over a 180° sample rotation at detector-to-sample distances of 7, 29, 59, and 119 mm.

The HT approach used in the present work differs from conventional x-ray microtomography based on attenuation contrast. The effect of the sample on an x-ray beam going through it is described by the refractive index $n = 1 - \delta + \iota\beta$, where δ is the refractive index decrement (typically approximately 10^{-6}), and β is the attenuation index. The fact that δ is much larger than the imaginary part β explains why the phase is more sensitive than the absorption. δ is actually proportional to the mean electron density, which is in turn nearly proportional to the mass density (also called physical density and expressed in mg/cm^3).

The imaging process leading to the 2D phase radiographs can be described as simple propagation, defocusing, or in-line holography and is done in two steps. In the first, the 2D distribution of the phase shift suffered by the beam is retrieved; in the present work, we use a method for phase retrieval that was recently experimented and described by Langer et al. [17]. In the second step, the 2D phase maps previously obtained are converted into a stack of 2D slices with the filtered back-projection algorithm. Thus, tomographic slices show the different physical densities of the analyzed samples. From the differences in densities, we can evaluate the degree of mineralization. Furthermore, in the 3D reconstructions it is possible to observe also the presence of new vessels and extracellular matrix (ECM), which are transparent in conventional attenuation-based tomographic reconstructions because of their low attenuation coefficients.

Statistical Analyses

For histomorphometry, the data are expressed as the means $\pm$ SD, and statistical analyses were performed with Student's test. A p value less than .05 was considered to be statistically significant.

For SR-HT data, statistical analyses were performed with SigmaStat 3.5 software (Systat Software Inc., Richmond, CA, http://www.systat.com). Statistical significance of all quantifications was assessed by two-tailed t test. p values were considered significant when $<.05$.

Results

Clinical and Radiographic Observations

Clinical assessment conducted 3 years after implantation of the mesenchymal stem cells/collagen biocomplexes did not reveal the presence of morbidity or infection at the intervention sites: functionality of mandibles was normal; no swelling or other alterations were observed; the mucosal membranes were normal; oral cavities were normal; and dental function, chewing, and quality of life were optimal. Above all, second molars were present and normal. All clinical observations on bone and dental structures near the area of repair indicated that there were no alterations. All analyses for the presence of viruses, routinely

performed before grafting and thereafter for the 3 years, were negative. Therefore, the clinical parameters were well balanced in all patients. However, clinical assessment of bone quality revealed that the regenerated (T) site was extremely hard with respect to the remaining mandible and particularly with respect to the contralateral (C) site. This was especially evident during the drilling of patients' mandibles to obtain biopsies: the operator had to apply much more force when drilling into T site bone (average of 36 N·cm for the T site, and an average of only 21 N·cm for the C site).

Radiographic analysis had revealed that, before grafting, the lower third molars were in close contact with the second molar roots (Fig. 1A) and that, after the operations, the depths of the defects were of the same dimensions on both sides (Fig. 1B). Six months after grafting, vertical regeneration was already visible, especially at the T sites (Fig. 1C). One year after interventions, bone regeneration was always greater at the T sites and was responsible for less exposure of the second molar roots here than at the C sites (Fig. 1D). Three years after surgery, T sites were completely regenerated and had better vertical bone height with respect to the C sites (Fig. 1E). In fact, probe-depth analysis revealed that the C sites presented with a mean gain of 4.5 ± 1.4 mm against a T site gain of 6.3 ± 2.1 mm ($p < .001$).

Hematoxylin-Eosin and Mallory's Trichrome Staining and Histomorphometric Analysis

Hematoxylin-eosin staining revealed that the collagen sponge used as the support component of the biocomplex was always completely reabsorbed and that there was bone regeneration at both the C and the T sites. However, human in vivo SC-treated mandible biopsies had a compact bone architecture, whereas human mandible control biopsies presented a cancellous (spongy) bone type. In particular, the regenerated bone at T sites was characterized by the presence of Haversian channels surrounded by lamellae (more than 20 in most cases), osteocyte-containing lacunae, and a high density of ECM (Fig. 2A). In contrast, the C sites were made up of interrupted lamellae surrounding numerous large marrow-filled spaces arranged in a more or less regular pattern (Fig. 2B). Mallory's Trichrome staining confirmed these findings (Fig. 2C, 2D).

Histomorphometric evaluation revealed that BV and BV/TV were significantly higher for human in vivo SC-treated mandible than for human mandible control, whereas BS/BV and MSV were significantly higher for human mandible control than for human in vivo SC-treated mandible (Table 1). This was consistent with the histological findings of a compact bone type at T sites and a cancellous bone type at C sites (Fig. 2).

Synchrotron Radiation-Based Holotomography

For SR-HT, the volume of interest considered was $895 \times 1{,}016 \times 1{,}376$ μm^3, divided into a stack of eight (172-μm-thick) voxel data sets in the vertical (z) direction (an example is given in Fig. 3A). The voxel data sets (32-bit float volumes per sample) were converted into the respective signed 8-bit data sets (gray scale from -128 to $+127$), and the distribution of gray values was analyzed with the software package VG Studio MAX 1.2 (Volume Graphics GmbH, Heidelberg, Germany, http://www.volumegraphics.com). In both the human mandible control and the human in vivo SC-treated mandible biopsies analyzed, the histogram could be formally divided into three sectors: the first (left-most), with an x value of <-50, represented a fully mineralized phase (i.e., high bone-mineral density); the second (middle) corresponded to not fully mineralized bone (i.e., a low bone-mineral density); and the third (right-most), with an x value of >0, represented unmineralized phases (air, cells, extracellular matrix, vessels, etc.) (Fig. 3B). This distribution can be explained by the fact that the gray levels were proportional to $-\delta$, the refractive index decrement. Moreover, the profile of the human in vivo SC-treated mandible biopsy was similar to that of the human mandible control: in fact, both had coexisting areas of mineralized and unmineralized tissue; however, the human in vivo SC-treated mandible biopsy presented an unexpectedly larger volume of bone, as revealed by the corresponding peak-integrated area.

In Figure 4, two representative subvolumes of human in vivo SC-treated mandible are shown: one, referring to the histological analysis, was used as a reference (Fig. 4A); the other is of the 3D reconstruction of the HT scan and the subsequent data analysis (Fig. 4B–4D). Two phases are represented in the HT images:

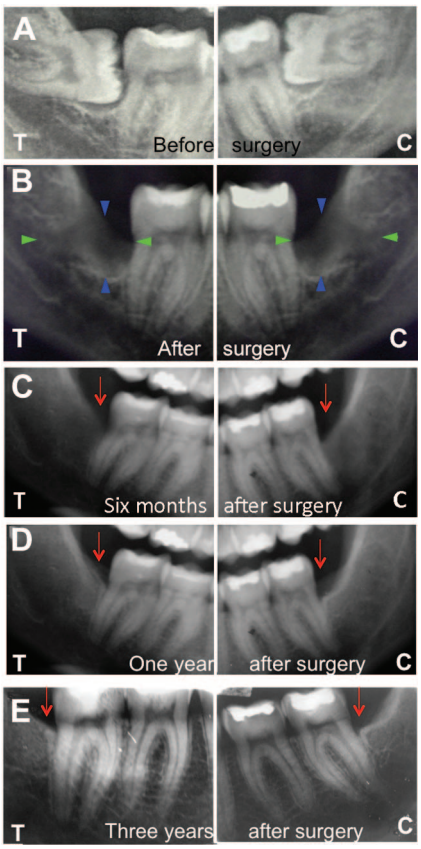

Figure 1. Representative x-ray radiographs of T and C sites in one patient before and after surgery. Radiographs were performed at the following time intervals: before surgery **(A)**, immediately after surgery **(B)**, 6 months after surgery **(C)**, 12 months after surgery **(D)**, and 3 years after surgery **(E)**. In **(A)**, the lower third molars can be seen in close contact with the second molar roots. In **(B)**, the depth of the defect, which is of the same dimensions on both sides, is clearly visible. The blue arrowheads indicate the vertical gap, while the green arrowheads show the horizontal gap. In **(C)**, a vertical regeneration more evident at the T site is already visible. One year after the intervention **(D)**, bone regeneration was greater at the T site; there was less exposure of the second molar root than at the C site. Three years after surgery **(E)**, the T site was completely regenerated, with better vertical bone height with respect to the C site. The red arrows indicate the cementum-enamel junctions. Abbreviations: C, control; T, test.

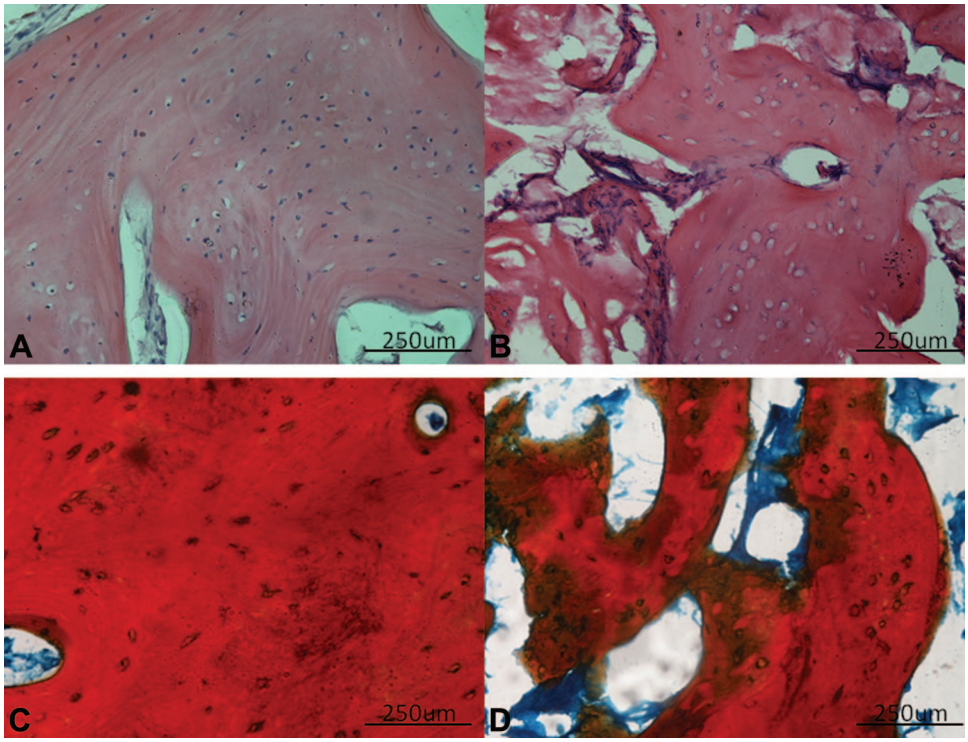

Figure 2. Histology of biopsies. **(A):** Representative hematoxylin-eosin staining of human in vivo stem cell (SC)-treated mandible sections revealed the presence of a compact bone architecture, characterized by Haversian channels surrounded by several lamellae. **(B):** In contrast, human mandible control biopsies were constructed from cancellous (spongy) bone, consisting in interrupted lamellae and numerous large spaces filled with marrow and arranged in a more or less regular pattern. **(C, D):** Mallory's trichrome staining confirmed the bone types present in human in vivo SC-treated mandible **(C)** and human mandible control **(D)**. Scale bars = 250 μm.

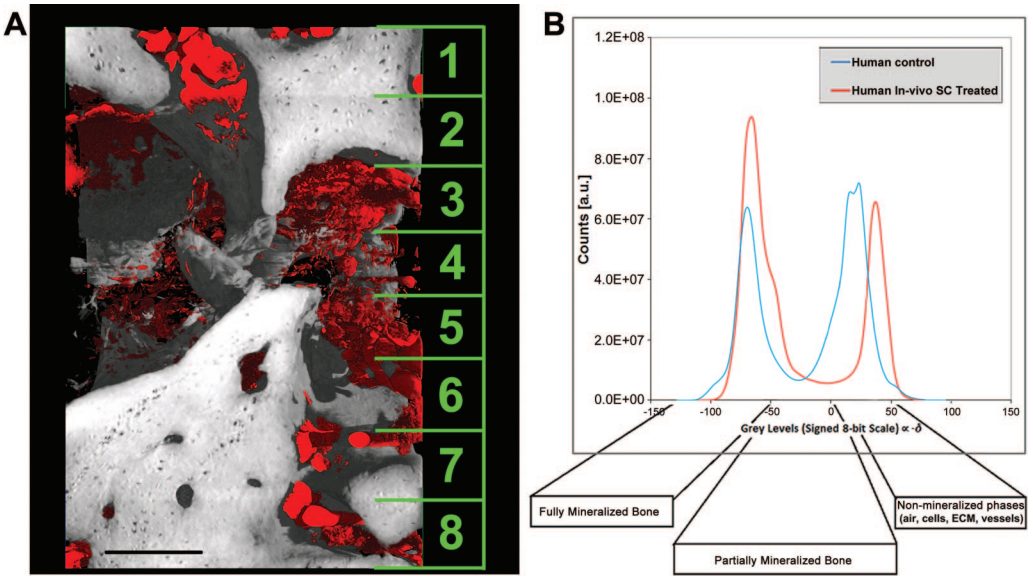

Figure 3. Synchrotron x-ray holotomography analysis. **(A):** Three-dimensional reconstruction for human control mandible showing the stack of eight voxel data sets. **(B):** Gray-value distribution histograms of the biopsies obtained from the test and control sites. Scale bar = 250 μm. Abbreviations: a.u., arbitrary units; ECM, extracellular matrix; SC, stem cell.

bone, independent of its degree of mineralization, and vessels (Fig. 4B–4D). One or more phases can be made translucent or can even be "canceled" in order to improve observation of the spatial distribution of the other phases. In Figure 4B, the unmineralized phase, except that representing vessels (visualized in red), has been deleted virtually to better visualize bone (in shades of gray) and its vascularization: the image demonstrates that in agreement with the histological analyses (Fig. 4A), after 3 years the bone tissue was well structured and vascularized. In Figure 4C, the vessel phase has been deleted virtually to better observe bone morphology: it is evident that bone regenerated after grafting was a compact-bone type. In Figure 4D, only densities compatible with the vessel phase have been visualized: there is clear evidence of good vascularization.

Table 1. Analyses of the constructs retrieved from in vivo grafts

	Test site (grafted)	Control	*p* value
Histomorphometric analysis			
BV (μm^3)	1.10 ± 0.3 ($\times 10^8$)	0.53 ± 0.31 ($\times 10^8$)	<.001
BS/BV (mm^{-1})	15 ± 1	32 ± 10	<.001
BS/TV (%)	79.8 ± 10.3	47.6 ± 7.6	<.01
MSV (%)	11.2 ± 2.3	52.3 ± 1.5	<.001
Three-dimensional holotomography-based morphometric analysis			
BV (μm^3)	1.10 ± 0.18 ($\times 10^8$)	0.49 ± 0.32 ($\times 10^8$)	.003
BS/BV (mm^{-1})	18 ± 6	55 ± 29	.004
BS/TV (%)	62.4 ± 11.7	24.8 ± 15.2	<.001
Mean BTh (μm)	119 ± 27	48 ± 29	.001
Mean BNr (mm^{-1})	5.3 ± 0.4	5.2 ± 0.9	.680
Mean BSp (μm)	70.1 ± 17.6	155.0 ± 61.2	.003

Abbreviations: BNr, bone number; BS, bone surface; BSp, bone spacing; BTh, bone thickness; BV, bone volume; MSV, marrow star space volume; TV, total volume.

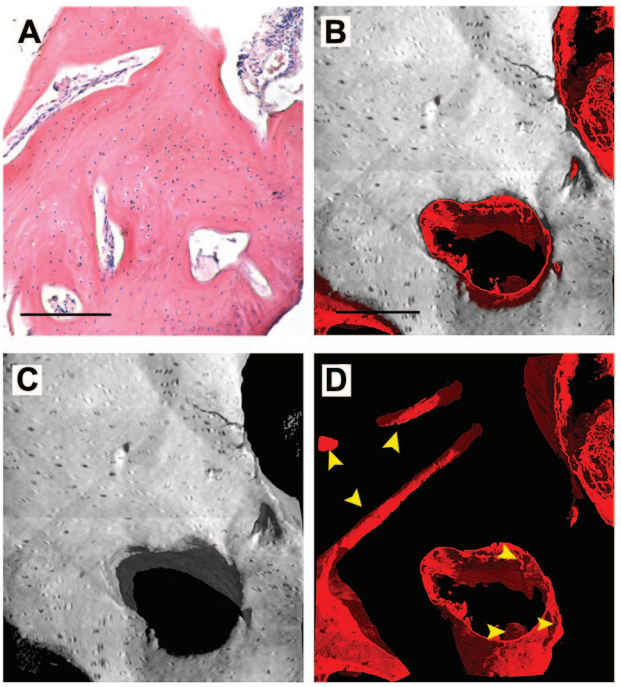

Figure 4. Three-dimensional images of human in vivo stem cell-treated mandible. **(A):** Histological section with hematoxylin-eosin staining, as a reference. **(B–D):** Subvolume of the three-dimensional (3D) synchrotron radiation-based holotomography reconstruction. To improve visualizations, in each 3D image all phases were deleted virtually, except for bone and vessels **(B)**, bone **(C)**, and vessels **(D)**. Yellow arrowheads indicate portions of vessels to distinguish them from possible artifacts. Scale bars = 250 μm.

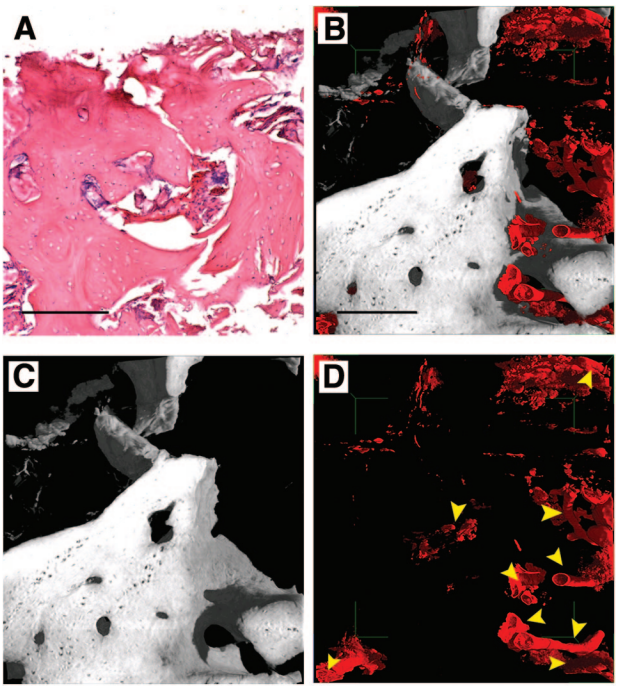

Figure 5. Three-dimensional (3D) images of human mandible control. **(A):** Histological section with hematoxylin-eosin staining, as a reference. **(B–D):** Subvolume of the 3D reconstruction from the holotomography investigation. To improve visualizations, in each 3D image all other phases were deleted virtually, except for bone and vessels **(B)**, bone **(C)**, and vessels **(D)**. Yellow arrowheads indicate vessels to distinguish them from possible artifacts. Scale bars = 250 μm.

This was repeated for the human mandible control (Fig. 5): it is evident that here the bone is a well-structured cancellous type (Fig. 5A–5C) and that it is homogeneously vascularized (Fig. 5D). In fact, a fully organized vessel network was observable in the human mandible control (Figs. 3A, 5D). Although vascularization seemed more extensive than in the human in vivo SC-treated mandible, density signals compatible with neo-vessels were found in several areas of the biopsy retrieved from the T site.

Morphometric analysis based on the eight voxel data sets from the human in vivo SC-treated mandible and the human mandible control is reported in Table 1. Consistent with histomorphometrical analysis, BV and BV/TV were significantly higher, and BS/BV was significantly lower, at the T site.

In order to assess whether the mass density of the bone (or bone-mineral density, BMD) was a stable and homogeneous parameter throughout the full 3D volume, the refractive index decrement profiles of all eight voxel data sets were computed for the human in vivo SC-treated mandible (Fig. 6A) and the human mandible control (Fig. 6B). The graphs clearly show that there are important differences between the two samples: whereas the human mandible control presented subvolumes characterized by highly negative refractive index decrements (i.e., strongly mineralized areas), the human in vivo SC-treated mandible had data sets with minor refractive decrements (i.e., areas with lower bone-mineral density). In fact, as reported in the stacked area charts (Fig. 6C, 6F), the human mandible control had high BMD areas (i.e., a signed 8-bit scale gray level < -60) that comprised from 60% to 80% of the total bone amount of each voxel data set; in contrast, the human in vivo SC-treated mandible had

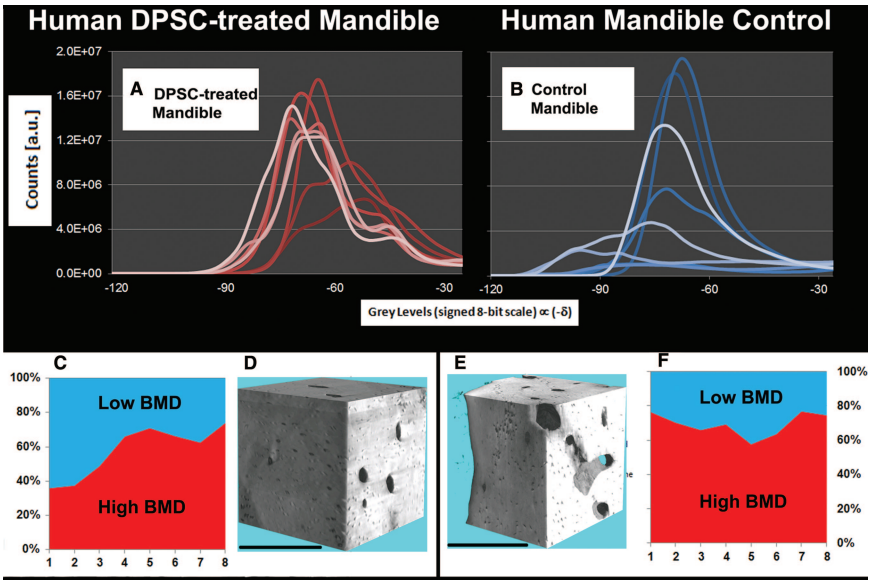

Figure 6. Bone density synchrotron radiation-based holotomography (SR-HT) analysis. **(A, B):** Gray value distribution for each voxel data set (represented by profiles with a different intensity of color) in the human in vivo stem cell (SC)-treated mandible and the human mandible control biopsy analyzed with SR-HT. **(C, F):** Percentage in each of the eight voxel data sets of the regions composed of high and low BMD. **(D, E):** Three-dimensional reconstructions of subvolumes of interest in the HT analysis of human in vivo SC-treated mandible **(D)** and human mandible control **(E)**. Scale bars = 250 μm. Abbreviations: a.u., arbitrary units; BMD, bone-mineral density; DPSC, dental pulp stem cell.

segments composed of as little as 40% high BMD. Although Student's *t* test of the mean percentages of high BMD in the eight voxel data sets revealed that there was no significant difference ($p = .066$), the mean percentage of high BMD in the human in vivo SC-treated mandible (57.7 $\pm$ 15.0%) had a larger (more than double) standard deviation with respect to that of the human mandible control (69.3 $\pm$ 6.7%). This fact suggests that the regenerated bone of the human in vivo SC-treated mandible had undergone an inhomogeneous mineralization process, as also shown in Figures 3B and 6A. This can be explained supposing either that the T sample had areas of lower stable mineralization (i.e., with a mineral composition resulting in a lower physical density, expressed as mg/cm^3) than the human mandible control or that there was partial remodeling in some areas of the human in vivo SC-treated mandible. Unlike with HT, which can define bone mineralization in mg/cm^3, there is no way of verifying the physical density of bone with histology. However, it was possible to verify an absence of osteoclasts by histology. This suggests that the areas with lower mineralization revealed by SR-HT in the human in vivo SC-treated mandible were not due to a remodeling processes but were the result of stable, local mineral balancing. Nonetheless, 3D reconstructions of two subvolumes, showing bone volume density (ratio of bone volume to total volume) (Fig. 6D, 6E), confirmed what was already observed comparing Figures 4C and 5C, that is, that human in vivo SC-treated mandible was composed of a more compact bone than the human mandible control, with a higher BV/TV caused by its conformation (i.e., presence of more than 20 lamellae) and an absence of marrow-containing lacunae typical of cancellous bone.

Discussion

Bone transplantation is a major strategy for the repair and reconstruction of bone defects [18]. However, reconstruction of the mandible has long been a difficult challenge for the oral and maxillofacial surgeon, at least up to now. The various methods that have been used include insertion of bone grafts, allogeneic materials, and vascularized free flaps [19]. However, none of the above is satisfactory: in fact, alloplastic materials carry the risk of bacterial infection and can perforate the skin or oral mucosa [20]; the harvesting of bone grafts is associated with morbidity and possible functional impairment at the donor site [21]; and the products used in some procedures can have costly, time-consuming manufacturing processes and controversial ethical issues [22].

Bone is continuously remodeled through specific osteoblast/osteoclast interaction [23]. However, the stem/progenitor cells residing in the periosteum and endosteum possess a limited regenerative potential [24]. In contrast, mesenchymal stem cells contained in dental pulp have a high differentiation potential [6, 25]. Therefore, we sought to study the bone regeneration process in injured human mandibles repaired with autologous DPSC/collagen sponge biocomplex implants [10]. We have reported here the situation in seven patients 3 years after the interventions.

After obtaining the initial data revealing that the regenerated bone had an unusual hardness and a nonphysiological architecture for the site, we performed histomorphometric analysis. This demonstrated, in a statistically significant way, that stem cells had regenerated a compact rather than a spongy bone type. At this point we were compelled to find more sophisticated, other than extremely reliable methods to assess our biopsies further. We reasoned that synchrotron radiation-based holotomography was appropriate because of its capability to deliver advanced characterization of samples, fully exploiting the sensitivity of phase-contrast imaging.

SR-HT can reconstruct 3D images and analyze tissues at resolutions comparable to histology. However, with respect to morphometric analyses conducted through histology, SR-HT generates additional and more reliable quantitative information because the whole 3D sample, rather than only selected 2D sections, is assessed [17]. This innovative technique allowed us not only to acquire qualitative and quantitative information on hard

tissue but also to assess the presence and distribution of unmineralized tissues (extracellular matrix, blood vessels, nerves, bone marrow, etc.) within the samples. Nevertheless, quantification of such unmineralized tissues by in-line HT is challenging because of the inherent limitations of the adopted method for phase retrieval. In fact, although the chosen algorithm for virtual reconstruction contends well with the low-frequency distortions that are often present in in-line HT reconstructions, it has the disadvantage of forcing the user to set the proportionality constant between attenuation and phase shifts only for a sole phase. We set this constant for bone, because the main goal of the study was to assess the performance of DPSCs in repairing mandible defects: this meant that δ values for soft tissues (which have quite high constants) were slightly underestimated.

We found that DPSCs loaded onto a collagen sponge and implanted into the space left after extraction of compacted molars regenerated a vascularized, compact bone: both histology and SR-HT conducted on biopsies retrieved 3 years from engraftment revealed that DPSCs had regenerated a lamellar bone type that was different from that of the biopsies retrieved from the control sites. The finding of a richly vascularized compact bone is similar to results obtained by grafting DSPCs in vivo in murine models [1, 3, 25]. However, DPSCs are able to differentiate into a fibrous bone type in vitro, as already demonstrated by us in long-term cultures, without the addition of osteogenic morphogens [3, 6, 7, 10]. Because the mandible is constructed from cancellous bone on account of its role linked to the presence of teeth and their movements, regeneration of a compact, rather than a spongy, bone type is difficult to justify physiologically. We conclude, therefore, that grafted DPSCs do not pursue the local environmental signals emanating from the alveolar bone surrounding the graft site. This must be taken into consideration to better understand stem cell behavior. On the other hand, it may be possible to obtain cancellous bone from hematopoietic stem cells associated with DPSCs.

Nonetheless, the procedure may be of clinical interest for several reasons: the regenerated bone seems to display better resistance, so it may be suitable for use in the elderly or in patients with bone reabsorption caused by disease; the presence of compact bone bestows more stability to the areas of the mandible affected and so may produce more favorable local conditions for dental implants; the regenerated bone may be more resistant to mechanical, chemical, physical, and pharmacological agents, such as biphosphonates responsible for mandible osteonecrosis and so may be useful in therapies for necrosis of the mandible. On this last point, it cannot be excluded that compact bone may better resist osteoclast attack because of the properties inherent in its structure: in fact, whereas osteoclasts can easily access sites of reabsorption in alveolar bone, because of the presence of large areas of marrow in close proximity to the matrix, this is more difficult in compact bone. We will assess this hypothesis in future studies.

Many patients have to think long and hard about the prospects of the surgical deformities of the face with respect to head and neck cancer before deciding whether to go with surgical treatment versus combination chemotherapy-radiation therapy. In this context, compact bone regenerated after DPSC engraftments in the mandible could be considered of fundamental importance in oral cancer treatment to limit the pathologic fracture and to guarantee a patient's life quality.

Conclusion

We have demonstrated the following: (a) Mesenchymal stem cells seeded on a collagen I scaffold actively and successfully repair bone. (b) Three years after grafting in mandibles, histological and in-line holotomography revealed that regenerated bone is uniformly vascularized and qualitatively a compact type, rather than a cancellous (spongy) type that is physiological for the area. (c) Most probably, regeneration of compact bone occurs because grafted dental-pulp stem cells do not follow the local signals of the surrounding spongy bone. This must be taken into consideration when grafting stem cells; their behavior may be quite variable, and consequently their differentiation fate in some cases may be affected more by their specific origin than by the local signals of the treated area. (d) In some clinical settings, the clinical advantages afforded by the grafting of autologous DPSCs may be more significant than the disadvantages arising from the regeneration of a bone type that is not normally present in the area treated.

Acknowledgments

This work, arising from a collaboration between COST NAMABIO partners (F.R., A.G., and G.P.), was supported by Second University of Naples Grant 2009-10 (to G.P.) and by European Union Grant P.O.N. (European Structural Funds for National Operating Programs) 01_02834 2011/14 (to G.P. and V.T.) for support with allocation of industrial ID19 Beamtime use at the ESRF (F). We sincerely thank Dr. Paul Tafforeau and Dr. Elodie Boller for their help at the ESRF during the x-ray holotomography experiments.

Author Contributions

A.G., A.M., and M.L.: performance of in-line HT experiments, interpretation of results, manuscript writing; F.R.: interpretation of HT results, manuscript revision; V.D. and F.P.: performance of experiments, data analysis; A.D.R., L.L., and R.d.A.: performance of clinical studies; V.T. and G.P.: planning of experiments, data collection and interpretation, manuscript writing, manuscript revision.

Disclosure of Potential Conflicts of Interest

The authors indicate no potential conflicts of interest.

References

1 Graziano A, d'Aquino R, Laino G et al. Human CD34+ stem cells produce bone nodules *in vivo.* Cell Prolif 2008;41:1–11.

2 Paino F, Ricci G, De Rosa A et al. Ectomesenchymal stem cells from dental pulp are committed to differentiate into active melanocytes. Eur Cell Mater 2010;20:295–305.

3 d'Aquino R, Graziano A, Sampaolesi M et al. Human postnatal dental pulp cells co-differentiate into osteoblasts and endotheliocytes: A pivotal synergy leading to adult bone tissue formation. Cell Death Differ 2007;14:1162–1171.

4 d'Aquino R, De Rosa A, Laino G et al. Human dental pulp stem cells: From biology to clinical applications. J Exp Zool B Mol Dev Evol 2009;312B:408–415.

5 d'Aquino R, Tirino V, Desiderio V et al. Human neural crest-derived postnatal cells exhibit remarkable embryonic attributes either in vitro or in vivo. Eur Cell Mater 2011;21:304–316.

6 Laino G, d'Aquino R, Graziano A et al. A new population of human adult dental pulp stem cells: A useful source of living autologous fibrous bone tissue (LAB). J Bone Miner Res 2005;20:1394–1402.

7 Laino G, Carinci F, Graziano A et al. In vitro bone production using stem cells derived from human dental pulp. J Craniofac Surg 2006;17: 511–515.

8 Tirino V, Paino F, De Rosa A et al. Identification, isolation, characterization, and banking of human dental pulp stem cells. Methods Mol Biol 2012;879:443–463.

9 Graziano A, d'Aquino R, Cusella-De Angelis MG et al. Scaffold's surface geometry significantly affects human stem cell bone tissue engineering. J Cell Physiol 2008;214:166–172.

10 d'Aquino R, De Rosa A, Lanza V et al. Human mandible bone defect repair by the grafting of dental pulp stem/progenitor cells and collagen sponge biocomplexes. Eur Cell Mater 2009;18:75–83.

11 Mangano C, De Rosa A, Desiderio V et al. The osteoblastic differentiation of dental pulp stem cells and bone formation on different titanium surface textures. Biomaterials 2010;31: 3543–3551.

12 Giuliani A, Frati C, Rossini A et al. High-resolution x-ray microtomography for three-dimensional imaging of cardiac progenitor cell homing in infarcted rat hearts. J Tissue Eng Regen Med 2011;5:e168–e178.

13 Cancedda R, Cedola A, Giuliani A et al. Bulk and interface investigations of scaffolds and tissue-engineered bones by X-ray microtomography and X-ray microdiffraction. Biomaterials 2007;28:2505–2524.

14 Giuliani A, Komlev V, Rustichelli F. Three-dimensional imaging by microtomography of x-ray synchrotron radiation and neutrons. In: Skrzypek JJ, Rustichelli F, eds. Innovative Technological Materials. Berlin, Germany: Springer-Verlag, 2010:123–177.

15 Cloetens P, Barrett R, Baruchel J et al. Phase objects in synchrotron radiation hard x-ray imaging. J Phys D Appl Phys 1996;29:133–146.

16 Cloetens P, Mache R, Schlenker M et al. Quantitative phase tomography of Arabidopsis seeds reveals intercellular void network. Proc Natl Acad Sci USA 2006;103:14626–14630.

17 Langer M, Cloetens P, Peyrin F. Regularization of phase retrieval with phase-attenuation duality prior for 3D holotomography. IEEE Trans Image Process 2010;19:2428–2436.

18 Khaled EG, Saleh M, Hindocha S et al. Tissue engineering for bone production- stem cells, gene therapy and scaffolds. Open Orthop J 2011;5:289–295.

19 Louis PJ. Bone grafting the mandible. Dent Clin North Am 2011;55:673–695.

20 Engstrand T. Biomaterials and biologics in craniofacial reconstruction. J Craniofac Surg 2012;23:239–242.

21 Pieske O, Wittmann A, Zaspel J et al. Autologous bone graft versus demineralized bone matrix in internal fixation of ununited long bones. J Trauma Manag Outcomes 2009;3:11.

22 Sukumar S, Drízhal I. Bone grafts in periodontal therapy. Acta Medica (Hradec Kralove) 2008;51:203–207.

23 Lemaire V, Tobin FL, Greller LD et al. Modeling the interactions between osteoblast and osteoclast activities in bone remodeling. J Theor Biol 2004;229:293–309.

24 Salgado AJ, Oliveira JT, Pedro AJ et al. Adult stem cells in bone and cartilage tissue engineering. Curr Stem Cell Res Ther 2006;1: 345–364.

25 Spath L, Rotilio V, Alessandrini M et al. Explant-derived human dental pulp stem cells enhance differentiation and proliferation potentials. J Cell Mol Med 2010;14:1635–1644.

See www.StemCellsTM.com for supporting information available online.